

Phonon-Magnon Interaction in Low Dimensional Quantum Magnets Observed by Dynamic Heat Transport Measurements

Matteo Montagnese,¹ Marian Otter,¹ Xenophon Zotos,² Dmitry A. Fishman,^{1,*} Nikolai Hlubek,³ Oleg Mityashkin,³ Christian Hess,³ Romuald Saint-Martin,⁴ Surjeet Singh,^{4,†} Alexandre Revcolevschi,⁴ and Paul H. M. van Loosdrecht^{1,‡}

¹Zernike Institute for Advanced Materials, Rijksuniversiteit Groningen, Nijenborgh 4, 9747 AG, The Netherlands

²Department of Physics, University of Crete and Foundation for Research and Technology-Hellas, 71003 Heraklion, Greece

³IFW-Dresden, Institute for Solid State Research, P.O. Box 270116, D-01171 Dresden, Germany

⁴Laboratoire de Physico-Chimie de L'Etat Solide, ICMMO, UMR8182, Université Paris-Sud, 91405 Orsay CEDEX, France

(Received 9 July 2012; published 4 April 2013)

Thirty-five years ago, Sanders and Walton [Phys. Rev. B **15**, 1489 (1977)] proposed a method to measure the phonon-magnon interaction in antiferromagnets through thermal transport which so far has not been verified experimentally. We show that a dynamical variant of this approach allows direct extraction of the phonon-magnon equilibration time, yielding 400 μ s for the cuprate spin-ladder system $\text{Ca}_9\text{La}_5\text{Cu}_{24}\text{O}_{41}$. The present work provides a general method to directly address the spin-phonon interaction by means of dynamical transport experiments.

DOI: [10.1103/PhysRevLett.110.147206](https://doi.org/10.1103/PhysRevLett.110.147206)

PACS numbers: 75.47.-m, 44.10.+i, 66.70.-f, 75.45.+j

Transport phenomena in condensed matter provide information on material excitations and their interactions that is not easily accessible by other methods [1]. In particular, they can be employed to study the interaction between spin and lattice excitations in magnetic materials. Spin-lattice coupling is of importance for many solid-state systems, influencing for instance the decoherence dynamics in molecular magnets [2], inducing the spin-Peierls instability of the spin-1/2 chains in the Mott insulator CuGeO_3 [3,4], and leading to some of the unusual properties found in multiferroic systems [5]. It also plays an important role in spin-transport phenomena, like in the recently discovered spin-Seebeck effect in magnetic insulators [6] and in the pumping of pure spin currents through the generation of coherent elastic waves [7]. While probing the magnetization dynamics provides information on spin-lattice coupling in ferromagnets, the array of experimental techniques offering direct access to the spin-phonon dynamics in antiferromagnets is limited, with pulsed electron spin resonance [8] as the most prominent example. Neutron scattering [9,10], Raman spectroscopy [11], and optical spectroscopy [12] provide indirect information only since disentangling the phonon-magnon dynamics from other, often dominant, scattering channels is usually not trivial.

Phonon-magnon coupling naturally plays an important role in the heat transport in magnetic materials. In fact, in a typical thermal transport experiment, only the phonon temperature can be directly accessed; the magnons contribute to the measured *effective* conductivity only through the interaction with the phonons. This argument, rationalized in the form of a two-temperature model [13,14] for the magnetic and phonon subsystems, has been used 35 years ago to qualitatively explain the large differences between the heat conductivities of certain three-dimensional magnetic materials [15]. In addition, the thermalization and diffusion

dynamics would induce an anomalous thickness dependence on the measured steady-state (dc) conductivities. However, a direct extraction of phonon-magnon coupling time in antiferromagnets using the proposed method has proven to be problematic due to the difficulty in measuring thin samples with conventional steady-state methods.

More recently, interest in magnetic heat transport has been revived due to the unusually large heat conductivities carried by magnetic excitations observed in low dimensional quantum magnets [16,17]. These antiferromagnetic materials show a variety of remarkable phenomena, including spin-liquid ground states [18] and the occurrence of dopant-bound spinon excitations near nonmagnetic impurities [19]. Whereas most of these phenomena are primarily of fundamental interest, their unusually large thermal conductivity may lead to applications in, among other areas, quantum information processing [20] and thermal management of electronic devices [21,22], partially explaining the revived interest. For infinite antiferromagnetic Heisenberg spin-chain (SC) materials, with their gapless topological magnon excitations (also called spinons), the large conductivity is understandable in terms of the theoretically expected ballistic magnetic heat transport along the chain axis [23]. Surprisingly, however, certain spin-ladder (SL) systems also show an exceptionally large thermal conductivity along the ladder [17], even though the transport by gapped magnon excitations is expected to be dissipative [24]. As discussed above, access to the magnetic heat transport depends crucially on phonon-magnon coupling, and it is therefore instrumental to measure and understand this coupling, not only in these intriguing low dimensional materials but also in other antiferromagnets.

This Letter addresses this issue by reporting room-temperature thermal conductivity measurements on the magnetically gapless SC SrCuO_2 and on the gapped SL

cuprate $\text{Ca}_9\text{La}_5\text{Cu}_{24}\text{O}_{41}$. Measurements have been performed using a steady-state method (SSM) and a dynamic time-domain fluorescent flash method (FFM). Surprisingly, the FFM thermal conductivity in the ladder direction $k_c^{\text{SL}}(\text{FFM})$ is found to be substantially lower than the one obtained by the SSM method (c is the ladder or chain axis). We interpret this discrepancy to be the signature of a large decoupling between the magnon and phonon subsystem in the SL, which combines with the defect-induced finite spin-ladder length to give an effective FFM thermal conductivity substantially lower than the static one. In addition, the SL compound also shows a much weaker dependence on the sample thickness than the SC compound, which we interpret in the framework of a much longer phonon-magnon thermalization time. We discuss these results in terms of suppression of the phonon-magnon scattering caused by the large two-magnon gap in the SL compound.

Single crystal platelets (thickness $L \approx 0.3\text{--}2.3$ mm) were cut and polished along different crystallographic axes from a single crystalline rod of $\text{Ca}_9\text{La}_5\text{Cu}_{24}\text{O}_{41}$ (SL compound) and SrCuO_2 (SC compound), which were grown by the traveling solvent floating zone technique [25]. For the FFM experiments [26], a thin layer of europium (III) thenoyltrifluoroacetate and deuterated Poly(methyl methacrylate) was spin coated on one side (the $x = L$ “front” side) of the samples. In the experiments, the second harmonic of a Q -switched Nd:YAG laser (532 nm, 10 ns pulse width) provided a heat pulse on the $x = 0$ “back” side, while a 360 nm LED was used to excite the europium (III) thenoyltrifluoroacetate layer on the front side. The resulting phosphorescence trace, detected by a GaAsP photodiode, is converted into a temperature

trace using calibration data, probing the temperature dynamics on the front surface resulting from the thermal excitation of the back surface. The values of $k(\text{FFM})$ are obtained from the diffusion coefficient by fitting the temperature dynamics with Parker’s formula [27], from which the sample diffusivity $k(\text{FFM})/C_p$ and the specific heat C_p can be independently extracted [28]. All FFM measurements were performed in air and at room temperature. In the SSM experiments, a heat current is applied by a resistive heater and the resulting temperature gradient is determined by measuring the temperature difference between the junctions of a differential Au/Fe-chrome thermocouple [29]. Thermal conductivities have been measured both along and perpendicular to the chain or ladder directions. Figure 1(a) presents the temperature-dependent static conductivities $k(\text{SSM})$ in the 5–300 K range. For both materials, the conductivity along the c axis (spin-chain or ladder direction) $k_c(\text{SSM})$ shows a magnetic contribution dwarfing the phonon component, producing a peak around 30 K for the SC and around 150 K for the SL [30].

The thickness-dependent FFM results along the c axis and the b axis, derived by fitting the temperature trace to Parker’s formula, are shown in Fig. 1(b). The results are plotted versus the b -axis phonon diffusion time [27] $\tau_d = 0.48 \frac{L^2 C_p}{\pi^2 k_b}$. Here, L is the sample thickness, and k_b is the (purely lattice-induced) conductivity along the b axis. The corresponding thickness scales are shown on the top axis for both the SC and SL samples. Perpendicular to the magnetic structures, $k_b(\text{FFM})$ data are in very good agreement with SSM data for both materials [31]. The dynamic conductivity along the c axis is more interesting. For the SC material $k_c^{\text{SC}}(\text{FFM})$ rapidly approaches a plateau

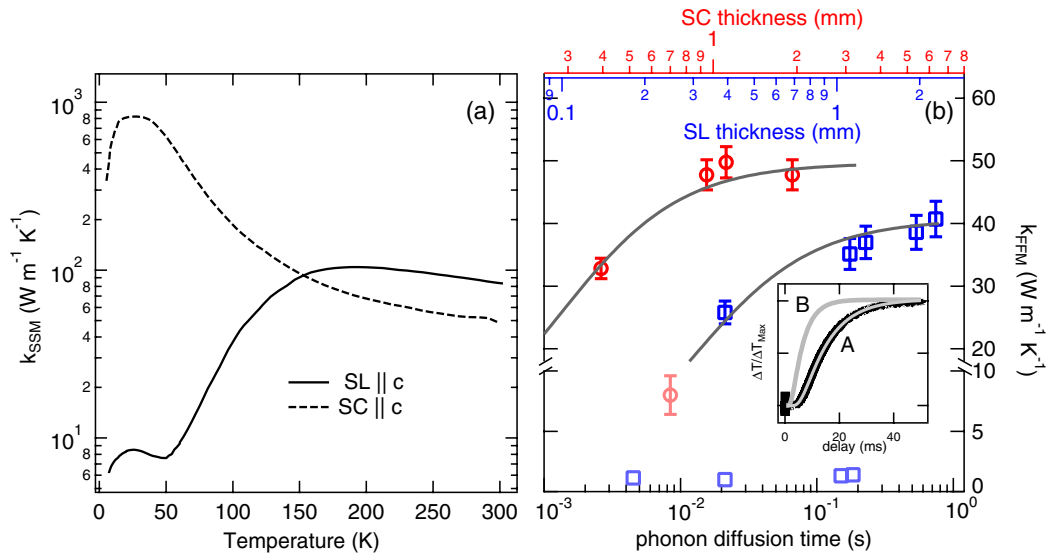


FIG. 1 (color online). (a) $k_c(\text{SSM})$ for the SC and the SL. (b) $k(\text{FFM})$ values for the SL (blue squares) and SC (red circles) along the c axis (solid texture) and the b axis (light texture). Data have been taken at 295 K. The results are plotted versus the phonon diffusion time τ_d (bottom axis; see the text) and the SC and SL thicknesses (top axes). The gray lines are guides for the eye. Inset: Trace A is a typical SL FFM temperature trace with a fitted Parker’s formula. Trace B is a simulation using $k_{\text{FFM}} = k_{\text{SSM}} = 85 \text{ W m}^{-1} \text{ K}^{-1}$.

corresponding to the SSM value of $50 \text{ W K}^{-1} \text{ m}^{-2}$ for $L > 1 \text{ mm}$. In the SL material, $k_c^{\text{SL}}(\text{FFM})$ data also approach a plateau, although in this case the final value of $\approx 42 \text{ W K}^{-1} \text{ m}^{-2}$ is roughly half that of the SSM value. This ‘‘SL anomaly’’ is also clearly observed by comparing a typical FFM temperature trace measured along the SL c axis [fitted value $k_c(\text{FFM}) \approx 35 \text{ W K}^{-1} \text{ m}^{-2}$] with the expected trace simulated using $k_c(\text{SSM}) \approx 85 \text{ W K}^{-1} \text{ m}^{-2}$ [inset of Fig. 1(b)]. As is clear from Fig. 1, both materials show a remarkable thickness dependence. More surprisingly, where for the SC material the data show a rapid convergence to the static value, the SL material $k_c^{\text{SL}}(\text{FFM})$ shows a much more gradual increase, which only for $L \approx 2 \text{ mm}$ approaches its limit value.

Temperature-dependent FFM measurements [32] show that the SL anomaly originates from the magnons since it disappears below 50 K along with the vanishing magnon contribution to the conductivity. At higher temperature, the SL anomaly can also be seen using other dynamic measurement methods such as the three-omega method [33] and the time resolved thermoreflectance [34]. We interpret the SL anomaly as a first and macroscopic signature that the spin-phonon coupling is much weaker in the SL than in the SC. This can be understood by considering that structural microdefects and chemical impurities effectively break the continuity of the spin structure (chain or ladder) in the single crystal samples. This results in an inhomogeneous magnetic heat transport in which the spin excitations have to scatter into phonons to bridge each structural defect and subsequently be reconverted back into spin excitations in the neighboring structure portion. By numerically modeling the SSM and FFM in the framework on the two component diffusion (see below) on a ‘‘broken’’ low dimensional quantum magnet sample, to simulate the presence of defects, we show that such dynamical retardation processes are more efficient in slowing down the thermal diffusion transients (measured by the FFM) than in quenching the equilibrium temperature gradient along the sample (measured by the SSM), with a larger effect the longer the phonon-magnon thermalization time of the spin structure is. This ultimately results in a reduced FFM magnetic conductivity [28].

We now focus on the thickness dependence, which provides more quantitative information on the phonon-magnon dynamics on a time scale comparable with τ_d and can be rationalized considering the details of the heat diffusion in the SC and SL materials. In particular, one realizes that (i) along the chain (ladder), heat is carried by phonons and SC (SL) magnons, diffusing across the sample as they undergo interconversion between each other, and (ii) in the SSM and FFM experiments, only the phonons are initially excited and subsequently probed. In fact, in the FFM experiment, one expects a high degree of nonequilibrium in the initial magnetic and lattice temperatures since the optical pulse illuminating the sample at time

zero creates high-energy electron-hole pairs that, through electron-phonon interactions, decay predominantly and quickly ($< 10 \text{ ps}$) into optical and acoustic phonons. The fast magnetic mode of heat transport is accessed only through phonon-magnon conversion, which occurs during diffusion through the sample. The energy exchange rate between the two systems can be described by a time constant τ_{mp} , which depends on the magnon and phonon distributions and on the details of the magnetoelastic coupling [13]. In addition, the Eu-TTA fluorescent layer on the sample front surface is sensitive to the local phonon temperature. Thus, as in the static case [15], in the FFM experiment, the magnon contribution to heat diffusion is detected mainly *because of* their coupling to the lattice. In this framework, the value of the measured, *effective* thermal conductivity is determined by the interplay between the phonon diffusion time τ_d and the phonon-magnon thermalization time τ_{mp} .

Let us consider a single magnetic mode coupled to the phonon bath. Two limit cases arise: If, for the given mode, $\tau_d \gg \tau_{mp}$, then heat is carried by the thermalized (magnon + phonons) system as a whole, giving rise to an effective thermal conductivity in which the magnetic contribution will simply add to the phonon contribution: $k_{\text{eff}} \approx k_l + k_m$. On the other hand, if $\tau_d \ll \tau_{mp}$, the magnon mode is thermally decoupled from the phonons, not partaking in the heat diffusion. Only the phonon contribution will be measured in this case: $k_{\text{eff}} \approx k_l$.

This analysis has been carried out theoretically for the SSM by Sanders and Walton [15], although the experimental implementation proved difficult. Using the FFM method, one can easily vary τ_d across some orders of magnitude by varying the sample thickness, allowing us to span between these two limiting cases in a controlled way. Within this framework, the total effective conductivity is given by the sum of the contributions of all the relevant magnetic modes to k_{eff} , their exact contribution depending on the thermalization time τ_{mp} .

The transport in these compounds can be described by a two-temperature (2T) model, obtained by phase space integration of the Bloch-Boltzmann-Peierls equation for the lattice (l , phonons) and magnetic (m , magnons) degrees of freedom [13,15]:

$$C_l \partial_t T_l = k_l \partial_x^2 T_l - g(T_l - T_m), \quad (1a)$$

$$C_m \partial_t T_m = k_m \partial_x^2 T_m + g(T_l - T_m). \quad (1b)$$

Here, t is time; x is the coordinate along the spin ladder or chain; $T_{l,m}$, $C_{l,m}$, and $k_{l,m}$ are the temperature, specific heat, and thermal conductivity for the lattice and the magnetic subsystems; and $g = C_m C_l / [(C_m + C_l) \tau_{mp}]$ is the coupling constant.

The 2T model can be analytically solved, and the solution can be fitted to the observed temperature evolution of the front side [28]. The parameter values used in this fitting are listed in Table I. The lattice conductivities, the SC

TABLE I. 2T model parameters used in the fitting of the FFM data and the resulting τ_{mp} .

Quantity	Spin ladder	Spin chain	Dimensions
k_l	1 ^a	8 ^a	$\text{W K}^{-1} \text{m}^{-1}$
k_m	45 ^b	40 ^a	$\text{W K}^{-1} \text{m}^{-1}$
C_l	2.86×10^{6a}	2.83×10^{6a}	$\text{J K}^{-1} \text{m}^{-3}$
C_m	1.5×10^{5c}	3×10^{4c}	$\text{J K}^{-1} \text{m}^{-3}$
Δ_{1M}	280 ^d		cm^{-1}
g (fitted)	1.5×10^9	2×10^{16}	$\text{W K}^{-1} \text{m}^{-3}$
τ_{mp}	$(4 \pm 1) \times 10^{-4}$	$(1 \pm 1) \times 10^{-12}$	s

^aSSM-measured values.^bFixed to half of the SSM value.^cCalculated values.^dReferences [31,35].

magnetic conductivity, and the total specific heats $C_m + C_l$ have been fixed to their experimental values at room temperature. For the SL material, k_m has been fixed to 0.53% of the SSM value due to the thermalization-defect interplay (see the discussion above). Indeed, the inhomogeneous sample problem can be mapped into a homogenous one, with the thermal parameters suitably renormalized from their intrinsic values since the presence of defects, to the first order, does not introduce any additional thickness dependence in the conductivity [28]. Finally, the magnetic specific heat for the SC compound has been determined experimentally [36], while the one for the SL compound has been calculated using the magnon dispersion [10]. This fixes all parameters in the model, except for the coupling constant g , globally fitted to the thickness-dependent data for both compounds.

Figure 2 presents the time-dependent data together with the fitted response. For the SC, we find a coupling constant $g \approx 2 \times 10^{16} \text{ W K}^{-1} \text{ m}^{-3}$, yielding $\tau_{mp} \approx (1 \pm 1) \times 10^{-12} \text{ s}$, indicating a thermalization time shorter than the sensitivity limits of the method. This result is largely determined by the $L = 0.4 \text{ mm}$ sample [see Fig. 1(b)]. Leaving out this data point leads to an even lower thermalization time.

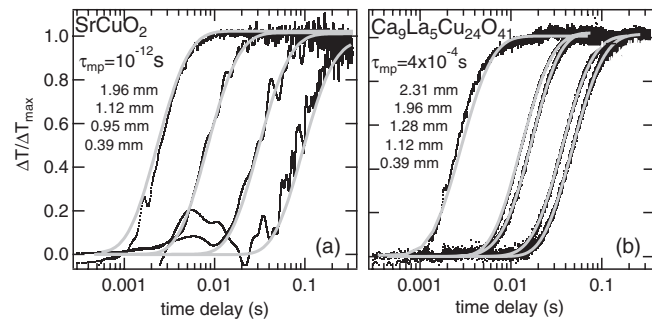


FIG. 2. (a) Normalized FFM temperature traces for the SC compound SrCuO₂ and (b) the SL compound Ca₉La₅Cu₂₄O₄₁ (black curves). The baseline temperature is 295 K. The leftmost (rightmost) curve corresponds to the thinnest (thickest) sample. The gray curves are the global fitting of the lattice solution of Eq. (1). The resulting thermalization times are also shown.

For the SL material, we find a coupling constant $g \approx 1.5 \times 10^9 \text{ W K}^{-1} \text{ m}^{-3}$. This corresponds to a thermalization time value of $\tau_{mp} \approx (4 \pm 1) \times 10^{-4} \text{ s}$, i.e., 8 orders of magnitude slower than in the SL case. This is one of the longest phonon-magnon thermalization times measured, comparable to those of 3D antiferromagnets (AFM) such as MnF₂, where electron spin resonance measurements give a spin-lattice relaxation $\tau_{\text{SL}} \approx 10^{-4} \text{ s}$ [15].

The much slower thermalization rates found in SL can be explained by considering (i) the details of the spin-phonon scattering, and in particular the role of *spin conservation* in determining the phase space available for the scattering process, and (ii) the *different energy overlap* between the magnetic and phonon dispersions, determined by the differences in the magnetic excitations of the SC and the SL. Because of spin conservation requirements, the magnetic and lattice subsystems interact via a two-spinon (or two-magnon) one-phonon scattering processes. The magnetic spectra and the relevant phonon states are shown in Fig. 3. For the SC [Fig. 3(a)], the boundaries of the gapless *two-spinon continuum* (2Sc) are [37] $\pi J/2 |\sin q| \leq \epsilon(q) \leq \pi J |\sin q/2|$, with the lower bound being the *single-spinon* (1S) dispersion. The AFM exchange parameter is $J = 1820 \text{ cm}^{-1}$ for SrCuO₂ [36]. In the SL, the interchain rung coupling hybridizes the two-chain spinon dispersions in a gapped triplet *one-magnon* (1M - $\Delta_{1M} = 280 \text{ cm}^{-1}$) and singlet *two-magnon* (2M - $\Delta_{2M} = 560 \text{ cm}^{-1}$) bound states [10,35]. The latter also delimits the *two-magnon continuum* (2Mc) in the first half ($[0, \pi/2]$) of the BZ. In this class of 1D AFM cuprates, the *c*-axis optical phonon has the highest magnetoelastic coupling with the chain or ladder magnetic modes. In particular, in the SL, the $\approx 500 \text{ cm}^{-1}$ A_g Cu-O stretching mode, strongly modulating the superexchange coupling, appears to be the main actor in the Lorenzana-Sawatzky phonon-mediated bimagnon light scattering [35]. It is worth

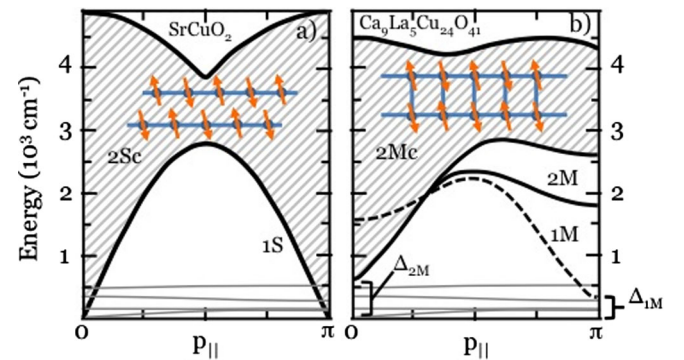


FIG. 3 (color online). Magnetic excitation spectra and phonon dispersions. In (a) SrCuO₂ (SC), the 2Sc (shaded area) crosses the low lying *c*-phonon bands (gray lines, from Ref. [38]) near the $q=0$ and $q=\pi$ Brillouin zone points, whereas, in (b) Ca₉La₅Cu₂₄O₄₁ (SL), the gap in the 1M bound state shifts the 2Mc above the phonon dispersion. The 2M bound state is also shown for completeness.

noting that, while the spin gap in the 1M state shifts the 2M and 2Mc dispersion above the phonon dispersion, the 2Sc dispersion has a sizable energy-momentum superposition with the relevant c -axis phonons, enhancing the phase space available for the transition, thereby reducing the phonon-magnon coupling time in the SL with respect to the SC.

In conclusion, we have measured the phonon-magnon decoupling in low dimensional antiferromagnets by means of dynamic heat conduction experiments. The present results directly confirm, almost 40 years after its proposal, the fundamental role of spin-phonon coupling in determining the observed thermal properties of magnetic materials. The slow phonon-magnon equilibration, with a time constant of 400 μ s, found for the spin-ladder material, finds its origin in the presence of a large spin gap, shedding light on the still not completely understood spin-lattice transport dynamics in low dimensional antiferromagnets. Moreover, the method presented here could be employed to study the spin-phonon coupling in classical three-dimensional antiferromagnets, as for instance MnF_2 [15].

We thank D. Cahill and M.C. Donker for fruitful discussions. This work was supported by the European Commission through the NOV MAG (FP6-032980) and LOTHERM (FP7-238475) projects and by the Deutsche Forschungsgemeinschaft through HE3439/7 and FOR 912 (HE3439/8). This research has also been co-financed by the ESF and Greek national funds through the Operational Program “Education and Lifelong Learning” of the NSRF under “Funding of proposals that have received a positive evaluation in the 3rd and 4th Call of ERC Grant Schemes.”

*Present address: Department of Chemistry, University of California at Irvine, Irvine, California 92697, USA.

†Present address: Indian Institute of Science Education and Research 900, NCL Innovation Park, Pune 411008, India.

‡P.H.M.van.Loosdrecht@rug.nl

- [1] M. Ziman, *Principles of the Theory of Solids* (Cambridge University Press, Cambridge, England, 1979).
- [2] S. Takahashi, I.S. Tupitsyn, J. van Tol, C.C. Beedle, D.N. Hendrickson, and P.C.E. Stamp, *Nature (London)* **476**, 76 (2011).
- [3] M.L. Hase, I. Terasaki, and K. Uchinokura, *Phys. Rev. Lett.* **70**, 3651 (1993).
- [4] C. Gros and R. Werner, *Phys. Rev. B* **58**, R14677 (1998).
- [5] A. Pimenov, A.A. Mukhin, V.Y. Ivanov, V.D. Travkin, A.M. Balbashov, and A. Loidl, *Nat. Phys.* **2**, 97 (2006).
- [6] K. Uchida, S. Takahashi, K. Harii, J. Ieda, W. Koshibae, K. Ando, S. Maekawa, and E. Saitoh, *Nature (London)* **455**, 778 (2008).
- [7] M. Weiler, H. Huebl, F.S. Goerg, F.D. Czeschka, R. Gross, and S.T.B. Goennenwein, *Phys. Rev. Lett.* **108**, 176601 (2012).
- [8] Y. Ajiro, *J. Phys. Soc. Jpn.* **72**, 12 (2003).
- [9] R.S. Eccleston, M. Uehara, J. Akimitsu, H. Eisaki, N. Motoyama, and S.I. Uchida, *Phys. Rev. Lett.* **81**, 1702 (1998).
- [10] S. Notbohm *et al.*, *Phys. Rev. Lett.* **98**, 027403 (2007).
- [11] P.E. Sulewski and S.-W. Cheong, *Phys. Rev. B* **51**, 3021 (1995).
- [12] S.A. Klimin, A.B. Kuzmenko, M.N. Popova, B.Z. Malkin, and I.V. Telegina, *Phys. Rev. B* **82**, 174425 (2010).
- [13] U.N. Upadhyaya and K.P. Sinha, *Phys. Rev.* **130**, 939 (1963).
- [14] B.H. Armstrong, *Phys. Rev. B* **23**, 883 (1981).
- [15] D.J. Sanders and D. Walton, *Phys. Rev. B* **15**, 1489 (1977).
- [16] A.V. Sologubenko, E. Felder, K. Giannò, H.R. Ott, A. Vietkine, and A. Revcolevschi, *Phys. Rev. B* **62**, R6108 (2000).
- [17] C. Hess, *Eur. Phys. J. Special Topics* **151**, 73 (2007).
- [18] H. Bethe, *Z. Phys.* **71**, 205 (1931).
- [19] G. Els, G.S. Uhrig, P. Lemmens, H. Vonberg, P. van Loosdrecht, G. Güntherodt, O. Fujita, J. Akimitsu, G. Dhahenne, and A. Revcolevschi, *Europhys. Lett.* **43**, 463 (1998).
- [20] S. Bose, *Phys. Rev. Lett.* **91**, 207901 (2003).
- [21] M. Pervolaraki, G. Athanasopoulos, R. Saint-Martin, A. Revcolevschi, and J. Giapintzakis, *Appl. Surf. Sci.* **255**, 5236 (2009).
- [22] M. Otter *et al.*, *Int. J. Heat Mass Transfer* **55**, 2531 (2012).
- [23] X. Zotos, F. Naef, and P. Prelovsek, *Phys. Rev. B* **55**, 11029 (1997).
- [24] F. Heidrich-Meisner, A. Honecker, D.C. Cabra, and W. Brenig, *Phys. Rev. Lett.* **92**, 069703 (2004).
- [25] A. Revcolevschi, U. Ammerahl, and G. Dhahenne, *J. Cryst. Growth* **198–199**, 593 (1999).
- [26] M. Otter, V.V. Krasnikov, D.A. Fishman, M.S. Pshenichnikov, R. Saint-Martin, A. Revcolevschi, and P.H.M. van Loosdrecht, *J. Magn. Magn. Mater.* **321**, 796 (2009).
- [27] W. Parker, R.J. Jenkins, C.P. Butler, and G.L. Abbott, *J. Appl. Phys.* **32**, 1679 (1961).
- [28] See Supplemental Material at <http://link.aps.org/supplemental/10.1103/PhysRevLett.110.147206> for details about fitting models and numerical simulations.
- [29] C. Hess, B. Büchner, U. Ammerahl, and A. Revcolevschi, *Phys. Rev. B* **68**, 184517 (2003).
- [30] N. Hlubek, P. Ribeiro, R. Saint-Martin, A. Revcolevschi, G. Roth, G. Behr, B. Büchner, and C. Hess, *Phys. Rev. B* **81**, 020405 (2010).
- [31] C. Hess, C. Baumann, U. Ammerahl, B. Büchner, F. Heidrich-Meisner, W. Brenig, and A. Revcolevschi, *Phys. Rev. B* **64**, 184305 (2001).
- [32] M. Montagnese (to be published).
- [33] G.I. Athanasopoulos, E. Svoukis, Z. Viskadourakis, and J. Giapintzakis, in *Thermal Conductivity 30/Thermal Expansion 18*, edited by D.S. Gaal and P.S. Gaal (DEStech Publications, Lancaster, 2010), p. 823.
- [34] D. Cahill (private communication).
- [35] M. Windt *et al.*, *Phys. Rev. Lett.* **87**, 127002 (2001).
- [36] I.A. Zaliznyak, H. Woo, T.G. Perring, C.L. Broholm, C.D. Frost, and H. Takagi, *Phys. Rev. Lett.* **93**, 087202 (2004).
- [37] J. des Cloizeaux and J.J. Pearson, *Phys. Rev.* **128**, 2131 (1962).
- [38] M.V. Abrashev, A.P. Litvinchuk, C. Thomsen, and V.N. Popov, *Phys. Rev. B* **55**, 9136 (1997).